SCIENTIFIC REPORTS

OPEN

SUBJECT AREAS:
LIGHT HARVESTING
PHOTOCATALYSIS
RENEWABLE ENERGY
TWO-DIMENSIONAL MATERIALS

Received
12 April 2013

Accepted
11 June 2013

Published
26 June 2013

Correspondence and requests for materials should be addressed to H.S.-J. (hwangsju@ewha.ac.kr)

Highly Efficient Visible Light-Induced O_2 Generation by Self-Assembled Nanohybrids of Inorganic Nanosheets and Polyoxometalate Nanoclusters

Jayavant L. Gunjakar, Tae Woo Kim, In Young Kim, Jang Mee Lee & Seong-Ju Hwang

Center for Intelligent Nano-Bio Materials (CINBM), Department of Chemistry and Nano Sciences, Ewha Womans University, Seoul 120-750, Korea.

Unusually high photocatalytic activity of visible light-induced O_2 generation can be achieved by electrostatically-derived self-assembly between exfoliated Zn-Cr-LDH 2D nanosheets and POM 0D nanoclusters ($W_7O_{24}^{6-}$ and $V_{10}O_{28}^{6-}$) acting as an electron acceptor. This self-assembly can provide a high flexibility in the control of the chemical composition and pore structure of the resulting LDH-based nanohybrids. The hybridization with POM nanoclusters remarkably enhances the photocatalytic activity of the pristine Zn-Cr-LDH, which is attributable to the formation of porous structure and depression of charge recombination. Of prime interest is that the excellent photocatalytic activity of the as-prepared Zn-Cr-LDH-POM nanohybrid for visible light-induced O_2 generation can be further enhanced by calcination at 200 °C, leading to the very high apparent quantum yield of ~75.2% at 420 nm. The present findings clearly demonstrate that the self-assembly of LDH–POM is fairly powerful in synthesizing novel LDH-based porous nanohybrid photocatalyst for visible light-induced O_2 generation.

The photoinduced generation of H_2 and O_2 molecules by semiconductor photocatalysts attracts a great deal of research activity because of its usefulness to harness solar energy and to transform it to user-friendly chemical energy[1–5]. Yet most of photocatalysts ever-developed do not possess a sufficiently high efficiency for visible light-induced production of O_2 gas because of their non-optimized band structure with wide bandgap energy and the mismatched position of valence band (VB). To achieve high photocatalytic activity of the visible light-induced O_2 generation, it is of crucial importance to finely tune several electronic characteristics of photocatalysts such as bandgap energy, band position, the lifetime of electron and hole, etc[3,6,7]. One of the most effective ways to tailor the band structure of inorganic solids is to control their chemical composition[8–12]. A facile tailoring of the electronic structure via chemical substitution renders layered double hydroxide (LDH) a promising candidate for photocatalytic O_2 generation and CO_2 conversion[13–19]. In particular, Zn-Cr-LDH material receives prime attention because of its unusually high efficiency for visible light-induced O_2 production[15]. Actually this LDH phase is one of the most active visible light photocatalysts for O_2 generation. In addition to the control of chemical composition, the hybridization with other semiconducting species is also fairly effective in optimizing the photocatalytic activity of the LDH materials through an expansion of the wavelength region of light absorption and an increase of electron–hole lifetime[14,15,19]. Taking into account the fact that negatively charged polyoxometalate (POM) nanocluster can act as an effective electron acceptor for positively charged LDH nanosheets via a strong electrostatic interaction[20–25], the hybridization with POM species can provide a powerful way of further enhancing the photocatalytic activity of the Zn-Cr-LDH phase. Under the irradiation of UV or visible light, the POM nanoclusters hybridized with the LDH nanosheets can accept photoexcited electrons from the conduction band (CB) of hybridized LDH lattice, leading to the formation of reduced POM* species[26–29]. The reduced POM* species can be readily reoxidized to the initial POM state via several oxidative pathways, which makes possible the role of POM nanocluster as an effective reversible redox shuttle (i.e. an electron transfer mediator). In addition to the enhancement of charge separation, the self-assembly with POM 0D nanoclusters can induce the surface expansion of the LDH material via the formation of porous intercalation structure, which is also beneficial for the photocatalyst performance of the resulting nanohybrids. In comparison with conventional ion-exchange route[20,21], the self-assembly process between exfoliated inorganic 2D nanosheets with

subnanometer-level thickness and 0D inorganic nanoclusters with very limited molecular dimension (~1 nm) would be much more effective in achieving a strong electronic coupling between these two semiconductors as well as in maximizing the surface area of the layered material via the formation of porous stacking structure[11,12,24,30–33]. To the best of our knowledge, there is however no report on the synthesis of self-assembled hybrid-type photocatalyst composed of exfoliated LDH 2D nanosheets and POM 0D nanoclusters.

In the present work, unusually high photocatalytic activity for visible light-induced O_2 generation can be achieved by a self-assembly between cationic Zn-Cr-LDH 2D nanosheets and anionic POM ($V_{10}O_{28}^{6-}$ and $W_7O_{24}^{6-}$) 0D nanoclusters. The effects of hybridization with POM on the photocatalytic activity and the surface area of the pristine Zn-Cr-LDH material are investigated together with the accompanying variations of their crystal structure and physicochemical properties. A strong electronic coupling with POM leads to the remarkable enhancement of the photocatalytic activity of the pristine Zn-Cr-LDH by ~4 times.

Results

To probe the effect of chemical formula on the physicochemical properties of the resulting nanohybrid materials, two different molar ratios of POM/Zn-Cr-LDH (i.e. a charge-balanced ratio and a 3-fold POM excess ratio) were applied for each POM species. The obtained self-assembled Zn-Cr-LDH–$W_7O_{24}^{6-}$ nanohybrids with a charge-balanced ratio (POM:Zn-Cr-LDH = 1 : 2.57) and a 3-fold POM-excess ratio (POM:Zn-Cr-LDH = 1 : 7.71) are denoted as **ZCW-1** and **ZCW-2**, respectively. Similarly the Zn-Cr-LDH–$V_{10}O_{28}^{6-}$ nanohybrids are denoted as **ZCV-1** and **ZCV-2** with the molar ratio of POM:Zn-Cr-LDH = 1 : 1.81 and 1 : 5.64, respectively. The powder XRD patterns of the as-prepared **ZCW** and **ZCV** nanohybrids and their calcined derivatives at 200°C are plotted in Fig. 1a, as compared to that of the pristine Zn-Cr-LDH. The pristine Zn-Cr-LDH material shows typical Bragg reflections of hexagonal LDH phase with interlayer nitrate ions, confirming the formation of Zn-Cr-LDH–nitrate phase. Like the pristine Zn-Cr-LDH, all of the present Zn-Cr-LDH–POM nanohybrids exhibit a series of well-defined (*00l*) Bragg reflections at low 2θ region, indicating the formation of layer-by-layer-ordered intercalation compound. All of the (*00l*) reflections of the pristine Zn-Cr-LDH are distinctly displaced toward low-angle side after the self-assembly with POM, clearly demonstrating the intercalation of POM nanoclusters in-between the host LDH lattice. For all the present nanohybrid materials, there is no distinct dependence of the basal spacing on the ratio of POM/LDH reactants, reflecting a high tolerance of the host LDH lattice for the variation of guest concentration. As illustrated in the right panel of Fig. 1b, the **ZCW** and **ZCV** nanohybrids possess expanded gallery heights of 1.06 and 1.20 nm, which is greater than that of the pristine Zn-Cr-LDH (0.89 nm). The in-plane (*110*) peak of hexagonal LDH phase and a broad hump peak are also observed at 2θ = ~60° and ~32–42° for all the present nanohybrids, respectively, underscoring the maintenance of the in-plane structure of the Zn-Cr-LDH nanosheets with disordered stacking structure.

The effect of heat-treatment on the crystal structure of the as-prepared Zn-Cr-LDH–POM nanohybrids is also examined with powder XRD analysis to estimate the thermal stability of these materials. As plotted in the right panel of Fig. 1a, even after the calcination at 200 °C, all the nanohybrids still display a series of (*00l*) reflections at low angle region as well as the in-plane (*110*) peak at high angle region, clearly demonstrating the maintenance of pillared structure up to 200 °C. The heat-treatment at 200 °C induces only a slight shift of (*00l*) peaks toward low angle side, suggesting the decrease of *c*-axis lattice parameter; the *c*-axis parameter of the calcined derivatives of **ZCW-1**, **ZCW-2**, **ZCV-1**, and **ZCV-2** nanohybrids is determined to be 0.95, 1.00, 1.08, and 1.14 nm, respectively. The observed shrinkage of basal spacing upon calcination is attributable to the evaporation of interlayer water molecules. A further elevation of heating temperature to 300 °C causes a remarkable depression of (*00l*) peaks, suggesting the destruction of intercalation structure (Supplementary Information, Fig. S1). Yet the in-plane peak of the LDH nanosheets as well as a broad hump at 2θ = 30–40° is still discernible for all the present materials calcined at 300 °C, indicating the maintenance of the Zn-Cr-LDH nanosheets even with the collapse of intercalation structure.

As illustrated in the left panel of Fig. 1b, cross-sectional HR-TEM analysis provides strong evidence for the formation of layer-by-layer-ordered intercalation structure for both the **ZCW** and **ZCV** nanohybrids. Both of the **ZCW-1** and **ZCV-1** nanohybrids display similar HR-TEM images showing the house-of-cards-type stacking structure of the heterolayered crystallites. The equally-spaced parallel lines corresponding to the layered lattice of Zn-Cr-LDH material are commonly observed for both the nanohybrid materials. From the enlarged views of the HR-TEM images, the distance between two consecutive fringes is determined to be ~1.0 and ~1.1 nm for the **ZCW-1** and **ZCV-1** nanohybrids, respectively. The estimated interline distances are in good agreement with the *c*-axis lattice parameters determined from the XRD analysis. The present HR-TEM images of the Zn-Cr-LDH–POM nanohybrids are very similar to those of self-assembled nanohybrids composed of exfoliated metal oxide 2D nanosheets and guest 0D nanoclusters[31–33]. The maintenance of the Zn-Cr-LDH nanosheets after the hybridization with POM and the following calcination is confirmed by X-ray absorption near-edge structure (XANES) analyses at Zn K- and Cr K-edge (Supplementary Information, Fig. S2 and Fig. S3). The local symmetry and oxidation state of guest POM nanoclusters in the present Zn-Cr-LDH–POM nanohybrids and their calcined derivatives are also examined using XANES analysis at W L_{III}-edge and V K-edge (Supplementary Information, Fig. S2 and Fig. S3).

The crystal morphology of the present Zn-Cr-LDH–POM nanohybrids is investigated with FE-SEM analysis. As presented in Fig. 1c, all of the as-prepared nanohybrids commonly exhibit porous morphology composed of house-of-cards-type stacking of sheet-like crystallites, strongly suggesting the presence of a large amount of mesopores in these materials. The house-of-cards-type stacking structure can be stabilized by the edge-to-face interaction of restacked LDH nanosheets. Such a mesoporous stacking structure is common for the self-assembled hybrid materials synthesized by the restacking of 2D nanosheets with 0D nanoclusters[17,34]. The heat-treatment at 200 and 300 °C has little influence on the highly anisotropic 2D shape of the LDH–POM nanohybrids, underscoring the high morphological stability of these materials. (Supplementary Information, Fig. S4).

According to energy dispersive spectrometry (EDS)-elemental mapping analysis (Supplementary Information, Fig. S5), all of the component elements, i.e. zinc, chromium, tungsten, vanadium, and oxygen, are uniformly distributed in entire parts of the as-prepared and calcined nanohybrids, clearly demonstrating the homogeneous hybridization of the Zn-Cr-LDH nanosheets and POM nanoclusters without any phase separation. The hybridization between Zn-Cr-LDH and POM is cross-confirmed by the EDS-line profile analysis, highlighting the homogeneous distribution of zinc, chromium, tungsten, vanadium, and oxygen elements along the line centered in the crystallites of the **ZCW-1** and **ZCV-1** nanohybrids (Supplementary Information, Fig. S6). Inductive coupled plasma (ICP) spectrometry and CHNS elemental analysis clearly demonstrate the tunability of the chemical composition of the Zn-Cr-LDH–POM nanohybrids synthesized by the self-assembly method (Supplementary Information). This sharply contrasts with the poor tunability of the chemical composition of the nanohybrids prepared by conventional ion-exchange method[22,23].

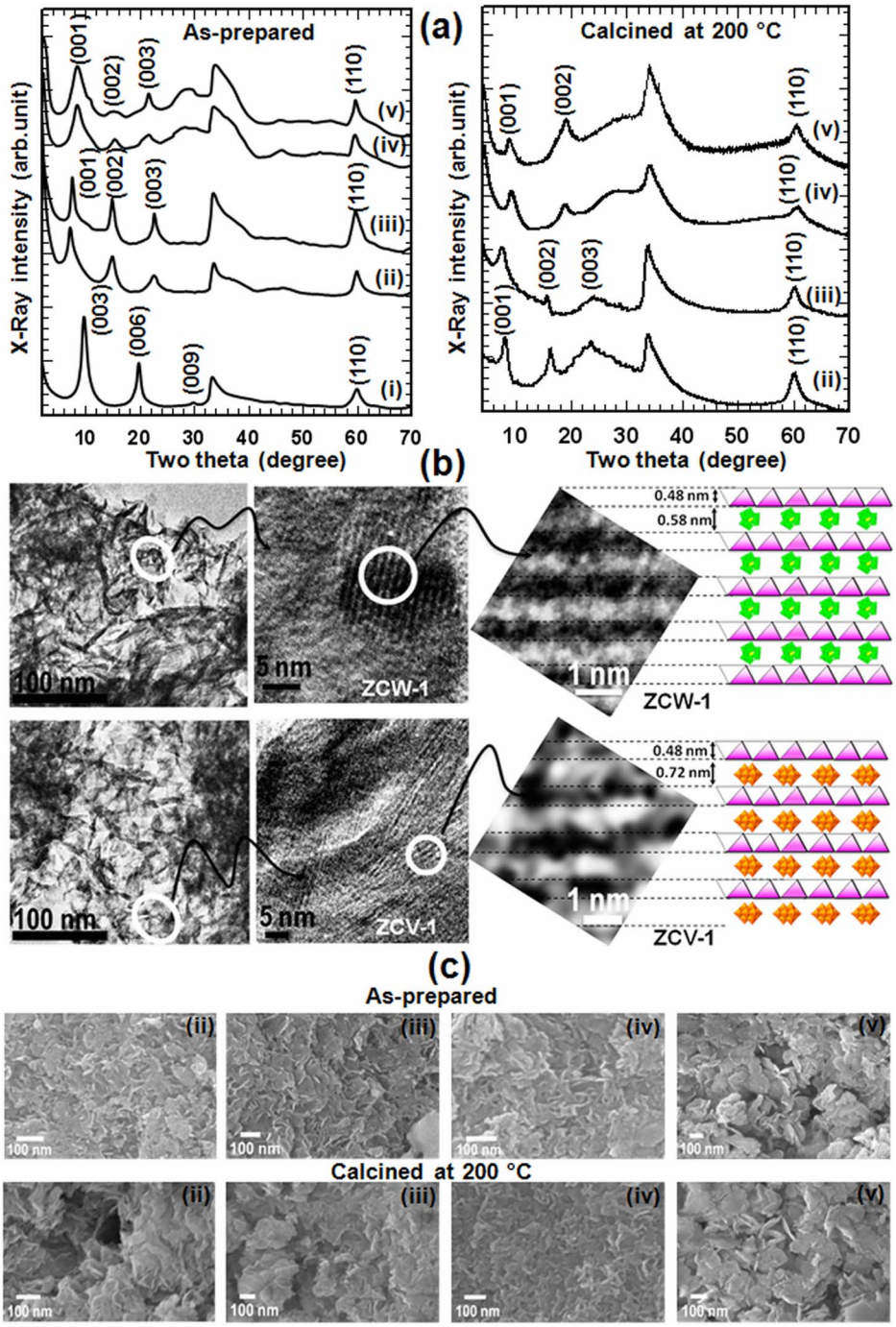

Figure 1 | Structural and microscopic study. (a) Powder XRD patterns of (i) the pristine Zn-Cr-LDH and the as-prepared nanohybrids of (ii) **ZCV-1**, (iii) **ZCV-2**, (iv) **ZCW-1**, and (v) **ZCW-2**. (b) Cross-sectional HR-TEM images of the **ZCW** and **ZCV** nanohybrids at high magnifications with (right) their schematic representation. (c) FESEM images of the as-prepared nanohybrids of (ii) **ZCV-1**, (iii) **ZCV-2**, (iv) **ZCW-1**, and (v) **ZCW-2**.

The pore structure and surface area of the present Zn-Cr-LDH–POM nanohybrids are investigated with N_2 adsorption–desorption isotherm measurements. As plotted in Fig. 2a, all of the as-prepared nanohybrids exhibit significant N_2 adsorption at $pp_0^{-1} < 0.4$. Since the adsorption of N_2 in the low pressure region occurs mainly on the micropores, the observed distinct N_2 adsorption in the region of $PP_0^{-1} < 0.4$ indicates the presence of micropores in the present materials. A distinct hysteresis is commonly observable for all the nanohybrids at $pp_0^{-1} > 0.45$, showing the presence of mesopores in the present materials. The observed isotherm and hysteresis behaviors can be classified as Brunauer–Deming–Deming–Teller (BDDT)-type-IV shapes and H2-type hysteresis loop in the IUPAC classification[35,36]. Such a combination of type IV isotherm and type H2 hysteresis is characteristic of mesoporous material having a high energy of adsorption and the presence of well-ordered pores with narrow and wide sections and interconnecting channels. This type of data reflect the presence of the open slit-shaped capillaries with very wide bodies and narrow short necks[36]. The heat-treatment at 200 and 300 °C causes a significant weakening of the hysteresis, indicating the partial destruction of mesoporous stacking structure at these temperatures (Supplementary Information, Fig. S7).

The surface areas of the present Zn-Cr-LDH–POM nanohybrids are calculated based on the Brunauer–Emmett–Teller (BET)

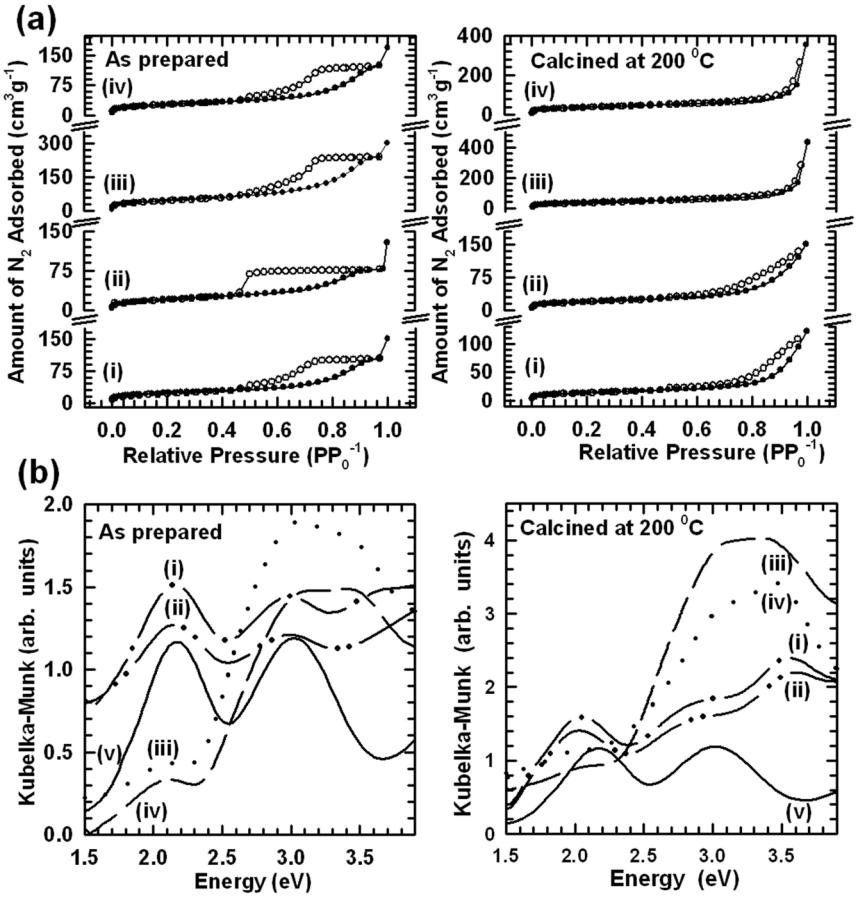

Figure 2 | N_2 Adsorption–desorption isotherms and optical properties. (a) N_2 adsorption–desorption isotherms and (b) diffuse reflectance UV-vis spectra of (i) **ZCW-1**, (ii) **ZCW-2**, (iii) **ZCV-1**, (iv) **ZCV-2** and (v) the pristine Zn-Cr-LDH.

equation. All of the as-prepared nanohybrids possess an expanded surface area of 167, 92, 86, and 74 m^2g^{-1} for **ZCV-1**, **ZCV-2**, **ZCW-1**, and **ZCW-2**, respectively, which is much greater than that of the pristine Zn-Cr-LDH (~25 m^2g^{-1}). This result underscores the usefulness of hybridization with POM nanoclusters in expanding the surface area of the LDH material[17]. Among the present materials, the **ZCV-1** and **ZCW-1** nanohybrids with lower POM contents have a greater surface area than do the **ZCV-2** and **ZCW-2** with higher POM contents. The observed dependence of surface area on the content of POM is attributable to the blocking of pores by the excess guest POM nanoclusters. For most of the present nanohybrids, the calcination at 200 and 300 °C induces the significant depression of the surface area, a result of the decrease of interlayer spacing and the partial destruction of pillared structure (Supplementary Information, Fig. S7). The decrease of surface area upon the heat-treatment is less prominent for the **ZCW-2** and **ZCV-2** nanohybrids with a higher POM/LDH ratio than for the **ZCW-1** and **ZCV-1** ones with a lower ratio, indicating the enhanced stability of the pillared structure by the intercalation of a larger amount of POM nanoclusters. In contrast to the present self-assembled Zn-Cr-LDH–polyoxotungstate nanohybrids, the homologue synthesized by ion-exchange method shows much smaller surface area of 35 m^2g^{-1}, clearly demonstrating the merit of self-assembly method in optimizing the pore structure of the resulting intercalative nanohybrid. According to the pore-size calculation based on Barrett–Joyner–Halenda (BJH) method (Supplementary Information, Fig. S8), all the present nanohybrids have mesopores with an average diameter of ~3–8 nm. A comparison of pore size with basal spacing indicates the mesopores in these materials are formed by the house-of-cards stacking structure of layered crystallites, not by intercalation structure.

The band structure and optical property of the as-prepared Zn-Cr-LDH–POM nanohybrids and their calcined derivatives are investigated with diffuse reflectance UV-vis spectroscopy. As plotted in Fig. 2b, the pristine Zn–Cr–LDH material shows two strong absorption peaks at ~2.2 and ~2.9 eV, which are assigned as the transition of Cr $3d_{t2g} \rightarrow$ Cr $3d_{eg}$ (transition) and the ligand-to-metal-charge-transfer (LMCT) of O $2p \rightarrow$ Cr $3d_{eg}$ of trivalent chromium ions, respectively[15]. The as-prepared **ZCV** nanohybrids display marked spectral difference from the optical profile of the pristine Zn-Cr-LDH material, a result of overlap between the *d*–*d* transitions of vanadium ions in the guest polyoxovanadate clusters and those of chromium ions in the host Zn-Cr-LDH lattice, see the left panel of Fig. 2b. Conversely, the UV-vis spectra of the **ZCW** nanohybrids are quite similar to that of the pristine Zn-Cr-LDH, which is attributable to the absence of the *d*–*d* transition of hexavalent tungsten ions in the polyoxotungstate species. Regardless of spectral change upon the hybridization with POM nanoclusters, all of the present nanohybrid materials display a strong absorption in visible light region, clearly demonstrating the visible light harvesting ability of these materials. The visible light absorption ability of the as-prepared nanohybrids is well-maintained after the heat-treatment at 200 and 300 °C (Supplementary Information, Fig. S9). The prominent visible light absorption by the **ZCW** and **ZCV** nanohybrids strongly suggests their potential applicability as visible light active photocatalysts.

Discussion

The charge transfer between Zn-Cr-LDH nanosheets and POM nanoclusters is investigated with PL spectroscopy. As plotted in the left panel of Fig. 3a, the PL signal of the pristine Zn-Cr-LDH becomes nearly quenched after hybridization with POM nanoclusters,

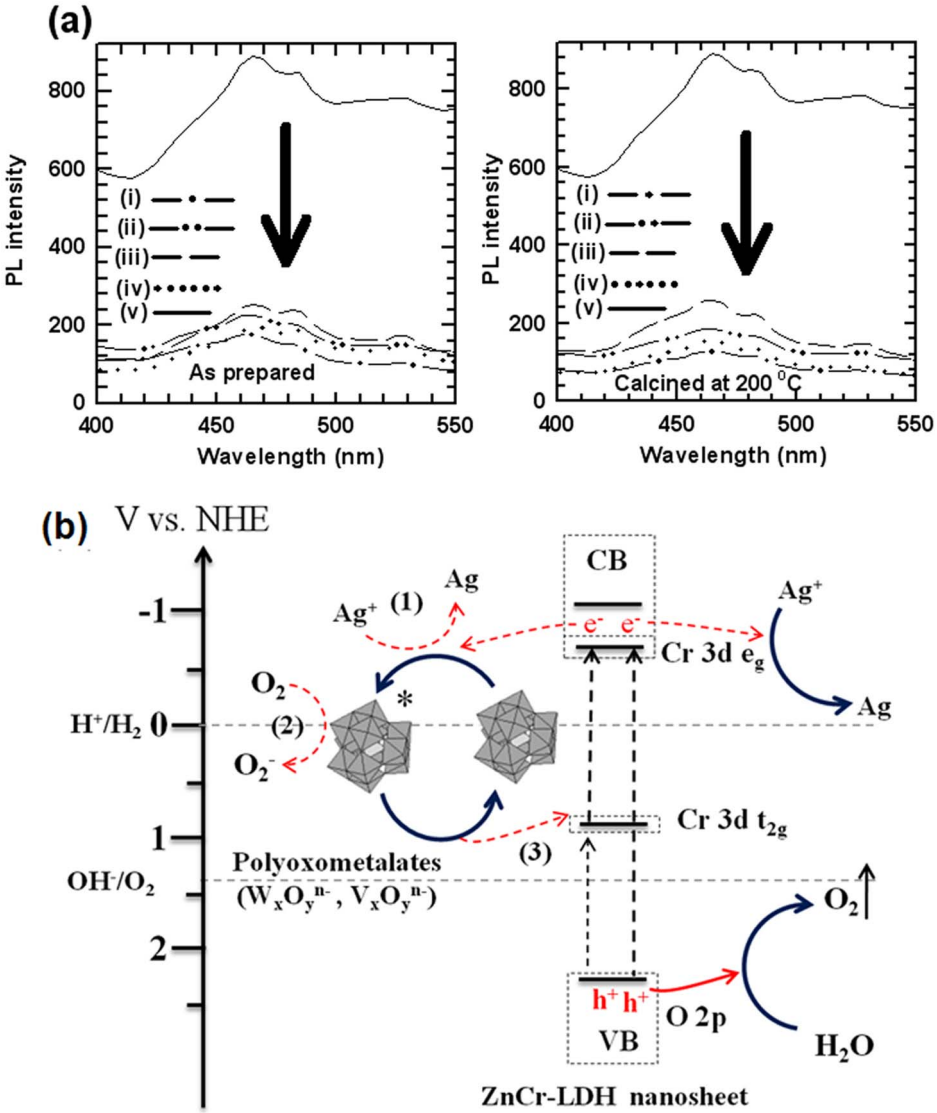

Figure 3 | PL spectroscopy and proposed charge transfer mechanism. (a) PL spectra of the **ZCW-1** (dot-dashed lines), **ZCW-2** (dot-dot-dashed lines), **ZCV-1** (dashed lines), **ZCV-2** (dotted lines), and pristine Zn-Cr-LDH (solid lines). (b) Schematic illustration for internal electron transfer in the present Zn-Cr-LDH–POM nanohybrids.

indicating a significant depression of electron–hole recombination. Between the two kinds of nanohybrids, the **ZCW** nanohybrids show weaker PL signals than do the **ZCV** nanohybrids, indicating more efficient electron coupling between polyoxotungstate and Zn-Cr-LDH. The PL signals of the as-prepared Zn-Cr-LDH–POM nanohybrids remain depressed after the heat-treatment at 200 and 300 °C (Supplementary Information, Fig. S10), reflecting the decrease of charge recombination rate. The observed remarkable decrease of PL signal provides straightforward evidence for a strong electronic coupling between Zn-Cr-LDH and POM, leading to the increase of the lifetime of electrons and holes. In comparison with previously reported nanohybrids of Zn-Cr-LDH–layered titanate[17], the present nanohybrids of Zn-Cr-LDH–POM demonstrate much stronger depression of PL signals after the hybridization. This observation underscores the more efficient role of the POM nanocluster than the layered titanate nanosheet in accepting photoinduced electrons from the hybridized LDH components. From these results, the present Zn-Cr-LDH-POM nanohybrids are expected to show a higher photocatalytic activity than the previously reported Zn-Cr-LDH–layered titanate nanohybrid and the pristine Zn-Cr-LDH compound[15,17].

The observed remarkable depression of PL peaks upon the hybridization with POM can be understood by the internal charge transfer between Zn-Cr-LDH and POM component, as illustrated in Fig. 3b. Taking into account the previously reported band structure of the Zn-Cr-LDH phase and redox potential of POM nanocluster[17], there occurs an effective electron transfer from the CB of Zn-Cr-LDH component to the unoccupied orbitals of POM component, yielding a reduced POM* nanocluster. This internal charge transfer process is highly effective in depressing the recombination of photoexcited electrons and holes via their separation in space, which is mainly responsible for the significantly reduced PL signal of the present Zn-Cr-LDH–POM nanohybrids. The POM nanoclusters can act as a role of electron transfer mediator since the reduced POM* nanoclusters can be easily reoxidized to the initial POM nanoclusters via electron transports through the following effective pathways in Fig. 3b; (1) POM* $\rightarrow Ag^+$, (2) POM* $\rightarrow O_2$, and (3) POM* $\rightarrow$ holes in partially occupied interband Cr $3d_{t2g}$ state.

The variation of the photocatalytic activity of Zn-Cr-LDH upon the hybridization with POM is investigated by monitoring time-dependent O_2 generation under the illumination of visible light ($\lambda \geq 420$ nm), see Fig. 4. As reported previously[15,17], the pristine

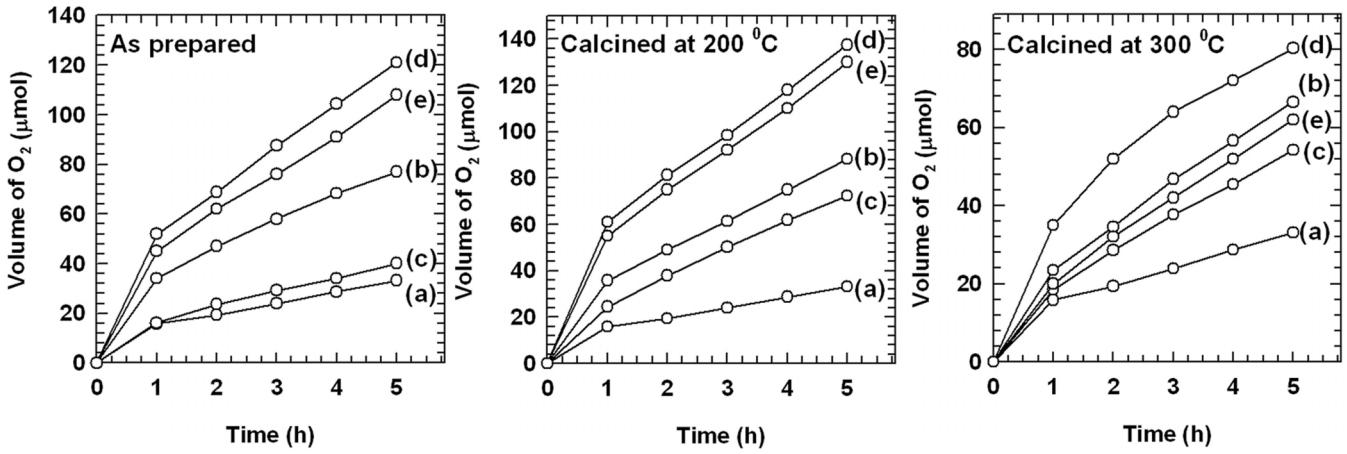

Figure 4 | Time-dependent photoproduction of O_2 gas under visible light illumination ($\lambda \geq 420$ nm). (a) the pristine Zn-Cr-LDH and the Zn-Cr-LDH–POM nanohybrids of (b) **ZCV-1**, (c) **ZCV-2**, (d) **ZCW-1**, and (e) **ZCW-2**.

Zn-Cr-LDH material shows high photocatalytic activity for visible light-induced O_2 generation, confirming its usefulness as photocatalyst for O_2 production. The as-prepared Zn-Cr-LDH–POM nanohybrids are much more active for the photocatalytic generation of O_2 molecules than the pristine Zn-Cr-LDH material, the pristine POM compounds, and their physical mixture (Supplementary Information, Fig. S11), highlighting the advantage of the hybridization with POM in improving the photocatalytic activity of the pristine Zn-Cr-LDH. The observed improvement of photocatalytic activity upon hybridization with POM nanoclusters is attributable to the effective electronic coupling between the two semiconductors (Zn–Cr–LDH and POM nanoclusters), leading to the increase of the lifetime of electrons and holes, as evidenced by PL measurements. Also the expansion of surface area upon hybridization with POM makes additional contribution to the observed improvement of photocatalytic activity through the provision of more reaction sites. The observed photocatalytic activity of the present Zn-Cr-LDH–POM nanohybrids is much higher than that of the previously reported Zn-Cr-LDH–layered titanate nanohybrids[19], highlighting the superior role of POM nanoclusters as a coupling agent for improving the photocatalytic activity of the pristine LDH material. Taking into account somewhat similar surface areas of the Zn-Cr-LDH–POM and Zn-Cr-LDH–layered titanate nanohybrids, the observed merit of the hybridization with POM nanoclusters is surely attributable to more effective internal electron transfer of LDH with POM than with layered metal oxide.

Among the present nanohybrids, the **ZCW** nanohybrids show much better photocatalytic activity than the **ZCV** homologues. The higher photocatalytic activity of the **ZCW** nanohybrids is attributable to the high photocatalytic activity of both Zn-Cr-LDH and polyoxotungstate for O_2 generation and also to the effective electronic coupling between the two components (Fig. 3)[15,17]. Additionally, the different molecular sizes of the polyoxovanadate and polyoxotungstate ($V_{10}O_{28}^{6-}$ and $W_7O_{24}^{6-}$) nanoclusters make additional contribution to the dissimilar photocatalytic activity of the **ZCV** and **ZCW** nanohybrids. As guessed from their molecular formulas, both of the POM nanoclusters possess different molecular sizes but the same molecular charge. Since the self-assembly between LDH and POM nanoclusters occurs in terms of electrostatic attraction, both of the **ZCV-1** and **ZCW-1** nanohybrids show nearly identical POM content, as evidenced by the inductive coupled plasma (ICP) analysis (Supplementary Information). Thus, the same number of the isovalent POM nanoclusters is supposed to bind with the specific surface area of Zn-Cr-LDH nanosheets both for the **ZCV-1** and **ZCW-1** nanohybrids. Taking into account the fact that the polyoxovanadate nanocluster ($V_{10}O_{28}^{6-}$) possesses markedly larger molecular size than does the polyoxotungstate nanocluster ($W_7O_{24}^{6-}$), the Zn-Cr-LDH nanosheet in the **ZCV-1** nanohybrid is supposed to have a greater surface coverage by the POM nanoclusters than the Zn-Cr-LDH nanosheet in the **ZCW-1** nanohybrid[37]. Since the visible light-induced O_2 generation occurs mainly on the surface of Zn-Cr-LDH, a severer surface blocking of Zn-Cr-LDH by the larger polyoxovanadate nanoclusters makes a significant contribution to the lower photocatalytic activity of the **ZCV-1** nanohybrid than the **ZCW-1** one. The suggested influence of the surface blocking of LDH nanosheets by the POM nanoclusters on the photocatalytic activity of the Zn-Cr-LDH–POM nanohybrids is supported by the fact that the **ZCW-1** and **ZCV-1** nanohybrids with lower POM contents show higher photocatalytic activity than the **ZCW-2** and **ZCV-2** nanohybrids with higher POM contents. In contrast to the **ZCW-1** and **ZCV-1** nanohybrids having similar POM contents, the **ZCW-2** and **ZCV-2** nanohybrids possess different POM contents. Since the latter materials have more POM nanoclusters for the specific surface area of the Zn-Cr-LDH nanosheets than do the former materials, they suffer from severer steric hindrance among the intercalated POM nanoclusters. As a consequence, the **ZCV-2** nanohybrid with larger polyoxovanadate nanoclusters shows a lower POM content than does the **ZCW-2** nanohybrid with smaller polyoxotungstate ions (Supplementary Information). Regardless of the POM contents, the surface of the Zn-Cr-LDH nanosheets in the **ZCW-2** and **ZCV-2** nanohybrids is more severely blocked by the POM nanoclusters compared with that in the **ZCW-1** and **ZCV-1** nanohybrids, leading to the degrading of their photocatalyst performance.

The effect of heat-treatment on the photocatalytic activity of the Zn-Cr-LDH–POM nanohybrids is also studied for the photoinduced generation of O_2 molecule. As presented in middle panel of Fig. 4, both the as-prepared **ZCV** and **ZCW** nanohybrids experience a significant improvement of their photocatalytic activity upon heat-treatment at 200 °C. In comparison with the as-prepared **ZCW-1** and **ZCV-1** nanohybrids, their derivatives calcined at 200 °C show even higher photocatalytic activity for visible light-induced O_2 evolution. The resulting photocatalytic activity of the **ZCW-1** nanohybrid calcined at 200 °C is 4 times higher than that of the pristine Zn-Cr-LDH material. The apparent quantum yield (AQY) of photocatalytic O_2 evolution is the most appropriate parameter to establish the photocatalytic efficiency. AQY for **ZCW-1** nanohybrid calcined at 200 °C is calculated to be 75.2% at wavelength 420 nm. Significant differences between experimental conditions adopted in the present study and in previous literatures make it difficult to directly compare the photocatalytic activity of the present self-assembled nanohybrids with those of other efficient photocatalysts ever-reported. However, taking into account the fact that the pristine Zn-Cr-LDH material is

one of the most effective photocatalysts for visible light-induced O_2 generation[15], the **ZCW** nanohybrid calcined at 200 °C can be evaluated as unusually highly active photocatalyst. A further elevation of heating temperature to 300 °C (right panel of Fig. 4) gives rise to the marked reduction of the photocatalytic activity of the present nanohybrids. This observation can be understood as a result of the significant decrease of surface area and the structural frustration of Zn-Cr-LDH nanosheets after the calcination at 300 °C. As can be seen from Fig. 4, all of the present nanohybrids display a higher photocatalytic activity for the initial stage of reaction than for the following stage after 1 h, which is attributable to the gradual consumption of sacrificial agent and also to the initial degradation of interlayer water molecules in-between the Zn-Cr-LDH layers. Similar time-dependence of photocatalyst performance is also reported for the pristine Zn-Cr-LDH material[15].

The photocatalytic activity of the Zn-Cr-LDH–polyoxotungstate nanohybrid prepared by the conventional ion-exchange route is also tested under the same condition, revealing much weaker photocatalytic activity than the self-assembled homologue. This result provides strong evidence for the advantage of the self-assembly method in optimizing the photofunctionality of LDH–POM nanohybrids. For consecutive three cycles, both the **ZCW-1** and **ZCV-1** nanohybrids retain most of photocatalytic activity (Supplementary Information, Fig. S12), clearly demonstrating the high stability of their photocatalytic activity. A slight decrease of photocatalytic activity is generally observed for the present materials like most of O_2-evolution photocatalysts, which is attributable to the masking of reaction sites by photodeposited Ag metal[15–17]. Even after the three-consecutive photoreactions, the crystal structure, crystal morphology, and chemical composition of the **ZCW-1** and **ZCV-1** nanohybrids remain nearly unchanged (Supplementary Information, Fig. S13), confirming the high structural and morphological stability of these materials.

In the present study, very efficient visible light-active photocatalysts for O_2 generation can be synthesized by the electrostatically-derived self-assembly between exfoliated Zn-Cr-LDH 2D nanosheets and an efficient electron acceptor of POM 0D nanoclusters, and the following heat-treatment at elevated temperature. The Zn-Cr-LDH–polyoxotungstate nanohybrid calcined at 200 °C shows unusually high photocatalytic activity for visible light-induced O_2 generation, which is 4 times higher than that of the pristine Zn-Cr-LDH. Considering that the pristine Zn-Cr-LDH phase is one of the most efficient visible light photocatalysts, the present Zn-Cr-LDH–POM nanohybrids with much higher photocatalytic activity must be one of the best photocatalyst materials for visible light-induced O_2 production. The remarkable enhancement of the photocatalytic activity of the pristine Zn-Cr-LDH upon the hybridization with POM is attributable not only to the formation of highly porous structure but also to the strong electronic coupling between the two components, leading to the depression of electron–hole recombination. In comparison with previously reported nanohybrid of Zn-Cr-LDH–layered titanate[19], the present Zn-Cr-LDH–POM nanohybrids are much more photocatalytically active because of the remarkable depression of charge recombination. Also the higher photocatalytic activity and the greater tunability of chemical composition of the self-assembled Zn-Cr-LDH–POM nanohybrid compared with the ion-exchanged homologue provide straightforward evidence for the merit of self-assembly method over the conventional ion-exchange method. The experimental findings presented here underscore that the self-assembly of LDH 2D nanosheets with electron accepting 0D nanoclusters can provide a very powerful way of developing highly efficient visible light active photocatalysts. This synthetic strategy based on the electrostatic interaction is readily extendible for diverse couples of cationic LDH nanosheets and anionic 0D nanoclusters. Currently we are underway to explore efficient visible light active photocatalysts from the self-assembly between photocatalytically active LDH 2D nanosheets and carbon 0D nanoclusters like fullerene species having a great electron accepting ability.

Methods

Preparation of Zn-Cr-LDH-POM nanohybrids. The nitrate form of Zn-Cr-LDH was synthesized by conventional co-precipitation method, as reported previously[17]. The dispersion of the pristine Zn-Cr-LDH powder in formamide yielded the colloidal suspension of exfoliated Zn-Cr-LDH nanosheets[17]. The self-assembled nanohybrids of **ZCW** and **ZCV** were prepared by the dropwise addition of the aqueous solution of POM anions ($W_7O_{24}^{6-}$ and $V_{10}O_{28}^{6-}$) to the formamide suspension of Zn-Cr-LDH nanosheets at room temperature. The formation of the self-assembled nanohybrids occurred just after the mixing of the two precursor solutions, verifying the rapid synthesis of the Zn-Cr-LDH–POM nanohybrids. Alternatively an attempt was made to synthesize the same material via conventional ion-exchange reaction. This reaction took more than 8 h to yield the crystalline Zn-Cr-LDH–polyoxotungstate nanohybrids, underscoring a much higher formation rate of the self-assembly route than that of the conventional ion-exchange one. The resulting nanohybrid materials were separated by centrifugation, washed with formamide and absolute ethanol, and finally vacuum-dried at 65 °C for 24 h. To prevent the contamination of the LDH materials with carbonate ions, all of the preparation processes in this work were carried out with decarbonated water under CO_2-free N_2 atmosphere.

Materials characterization. The crystal structures of the pristine Zn-Cr-LDH and the self-assembled nanohybrids of **ZCW** and **ZCV** were examined by powder X-ray diffraction (XRD) analysis using a Rigaku diffractometer with Ni-filtered Cu Kα radiation. The chemical compositions of these nanohybrids were analyzed with ICP (Shimazu ICPS-5000) and elemental CHNS analysis (CE-Instruments-EA-1110). The stacking structure between Zn-Cr-LDH and POM was probed by high resolution-transmission electron microscopy (HR-TEM) analysis using a Jeol (JEM 2100F) microscope at an accelerating voltage of 200 kV. For the HR-TEM measurement, the powdery nanohybrid samples were embedded in epoxy resin and sliced by an ultramicrotome. The surface morphology and elemental distribution of nanohybrids were studied with field emission-scanning electron microscopy (FE-SEM, Jeol JSM-6700F) equipped with energy-dispersive spectrometry (EDS)–elemental mapping analysis. X-ray absorption near edge structure (XANES) analysis was carried out at the beam line 10C of the Pohang Accelerator Laboratory (PAL) in Korea. The present XANES data were collected at room temperature in a transmission mode using gas-ionization detectors. All the present spectra at Zn K-edge, Cr K-edge, W L_{III}-edge, and V K-edge were calibrated by simultaneously measuring the spectrum of Zn, Cr, W, or V metal, respectively. The pore structure and surface area of the present nanohybrids were examined by measuring the N_2 adsorption–desorption isotherms at 77 K with a gas sorption analyzer (ASAP 2020). All the samples were degassed at 150 °C in a vacuum below 10^{-3} Torr for 4 h prior to adsorption measurements. The optical properties of the nanohybrids were investigated with diffuse reflectance UV-vis spectrometer (Sinco S-4100 spectrometer equipped with an integrating sphere 60 mm in diameter). $BaSO_4$ was used as a standard for the diffuse reflectance UV-vis spectra. Photoluminescence (PL) spectra were measured with Perkin-Elmer LS55 fluorescence spectrometer.

Photocatalytic O_2 evolution experiment. For the measurement of photocatalytically produced oxygen gas, 10 mg of the nanohybrid powder was dispersed in a quartz reaction cell using magnetic stirrer in 20 ml water, and then 0.01 M $AgNO_3$ was added as a sacrificial reagent. The head space of reactor was sealed with air tight silicon stopper, and the photocatalyst suspensions were thoroughly degassed using argon gas for 0.5 h. A 450 W Xe arc lamp (Newport) was used as a light source. Light was passed through a 10 cm IR water filter and a cut-off filter ($\lambda \geq 420$ nm for visible-light illumination) and then focused on the reactor. The light intensity of the oxygen evolution reactions was kept homogeneous up to 8 × 8 inch, and was adjusted with a Si solar cell (Fraunhofer Institute for Solar Energy System; Mono-SiCKG filter; Certificate No. C-ISE269) to AM 1.5 radiation (1 SUN, 1000 W/m²). In the course of O_2 evolution, the reactor and total assembly were kept in Ar-flowing environment. The amount of O_2 evolved was estimated by injecting 100 μl of reactor headspace gas into online gas chromatography (GC, Shimadzu GC-2014) after every hour. The apparent quantum yield was obtained from the percentage of the number of reacted electrons during O_2 evolution to the number of incident photons. The photon flux was monitored by inserting a band-pass filter ($\lambda = 420$ nm, FWHM = 10 nm) in front of the reaction cell.

1. Fujishima, A. & Honda, K. Electrochemical photolysis of water at a semiconductor electrode. *Nature* **238**, 37–38 (1972).
2. Lewis, N. S. & Nocera, D. G. Powering the planet: Chemical challenges in solar energy utilization. *Proc. Nat'l. Acad. Sci. USA* **103**, 15729–15735 (2006).
3. Kudo, A. & Miseki, Y. Heterogeneous photocatalyst materials for water splitting. *Chem. Soc. Rev.* **38**, 253–278 (2009).
4. Chen, X., Shen, S., Guo, L. & Mao, S. S. Semiconductor-based photocatalytic hydrogen generation. *Chem. Rev.* **110**, 6503–6570 (2010).
5. Zou, Z., Ye, J., Sayama, K. & Arakawa, H. Direct splitting of water under visible light irradiation with an oxide semiconductor photocatalyst. *Nature* **414**, 625–627 (2001).

6. Kudo, A. Recent progress in the development of visible light-driven powdered photocatalysts for water splitting. *Int. J. Hydrogen Energy* **32**, 2673–2678 (2007).
7. Lewis, N. S. Light work with water. *Nature* **414**, 589–590 (2001).
8. Shangguan, W. F. Hydrogen evolution from water splitting on nanocomposite photocatalysts. *Sci. Tech. Adv. Mater.* **8**, 76–81 (2007).
9. Zhang, L. L., Zhang, W. G., Lu, L. D., Yang, X. J. & Wang, X. Synthesis, structure and photocatalytic reactivity of layered $CdS/H_2La_2Ti_3O_{10}$ nanocomposites. *J. Mater. Sci.* **41**, 3917–3921 (2006).
10. Maeda, K., Higashi, M., Lu, D., Abe, R. & Domen, K. Efficient nonsacrificial water splitting through two-step photoexcitation by visible light using a modified oxynitride as a hydrogen evolution photocatalyst. *J. Am. Chem. Soc.* **132**, 5858–5868 (2010).
11. Kim, T. W. *et al.* Mesoporous iron oxide-layered titanate nanohybrids: soft-chemical synthesis, characterization, and photocatalyst application. *J. Phys. Chem. C* **112**, 14853–14862 (2008).
12. Kim, T. W. *et al.* Bifunctional heterogeneous catalysts for selective epoxidation and visible light driven photolysis: nickel oxide-containing porous nanocomposite. *Adv. Mater.* **20**, 539–542 (2008).
13. Teramura, K., Iguchi, S., Mizuno, Y., Shishido, T. & Tanaka, T. Photocatalytic conversion of CO_2 in water over layered double hydroxides. *Angew. Chem. Int. Ed.* **51**, 8008–8011 (2012).
14. Mohapatra, L., Parida, L. & Satpathy, M. Molybdate/Tungstate intercalated oxo-bridged Zn/Y LDH for solar light induced photodegradation of organic pollutants. *J. Phys. Chem. C* **116**, 13063–13070 (2012).
15. Gomes Silva, C., Bouizi, Y., Fornes, V. & Garcia, H. Layered double hydroxides as highly efficient photocatalysts for visible light oxygen generation from water. *J. Am. Chem. Soc.* **131**, 13833–13839 (2009).
16. Zhao, Y. *et al.* A family of visible-light responsive photocatalysts obtained by dispersing CrO_6 octahedra into a hydrotalcite matrix. *Chem. Eur. J.* **17**, 13175–13181 (2011).
17. Gunjakar, J. L., Kim, T. W., Kim, H. N., Kim, I. Y. & Hwang, S.-J. Mesoporous layer-by-layer ordered nanohybrids of layered double hydroxide and layered metal oxide: highly active visible light photocatalysts with improved chemical stability. *J. Am. Chem. Soc.* **133**, 14998–15007 (2011).
18. Zhao, Y., Wei, M., Lu, J., Wang, Z. L. & Duan, X. Biotemplated hierarchical nanostructure of layered double hydroxides with improved photocatalysis performance. *ACS Nano* **3**, 4009–4016 (2009).
19. Wang, H., Xiang, X. & Li, F. Hybrid ZnAl-LDH/CNTs nanocomposites: noncovalent assembly and enhanced photodegradation performance. *AIChE J.* **56**, 668–678 (2010).
20. Yun, S. K. & Pinnavaia, T. Layered double hydroxides intercalated by polyoxometalate anions with keggin (α-$H_2W_{12}O_{40}^{6-}$), dawson (α-$P_2W_{18}O_{62}^{6-}$), and finke ($Co_4(H_2O)_2(PW_9O_{34})_2^{10-}$) structures. *J. Inorg. Chem.* **35**, 6853–6860 (1996).
21. Drezdzon, M. A. Synthesis of isopolymetalate-pillared hydrotalcite via organic-anion-pillared precursors. *Inorg. Chem.* **35**, 4628–4632 (1988).
22. Weir, M. R. & Kydd, A. Synthesis of heteropolyoxometalate-pillared Mg/Al, Mg/Ga, and Zn/Al layered double hydroxides via LDH−hydroxide precursors. *Inorg. Chem.* **37**, 5619–5624 (1998).
23. Carriazo, D., Domingo, C., Martin, C. & Rives, V. Structural and texture evolution with temperature of layered double hydroxides intercalated with paramolybdate anions. *Inorg. Chem.* **45**, 1243–1251 (2006).
24. Kim, H. N. *et al.* Self-assembly of nanosized 0D clusters: CdS quantum dot-polyoxotungstate nanohybrids with strongly coupled electronic structures and visible-light-active photofunctions. *Chem. Eur. J.* **17**, 9626–9633 (2011).
25. Ma, R. & Sasaki, T. Nanosheets of oxides and hydroxides: ultimate 2D charge-bearing functional crystallites. *Adv. Mater.* **22**, 5082–5104 (2010).
26. Kim, S., Park, H. & Choi, W. Comparative study of homogeneous and heterogeneous photocatalytic redox reactions: $PW_{12}O_{40}^{3-}$ vs TiO_2. *J. Phys. Chem. B* **108**, 6402–6411 (2004).
27. Ozer, R. R. & Ferry, J. L. Investigation of the photocatalytic activity of TiO_2-polyoxometalate systems. *Environ. Sci. Technol.* **35**, 3242–3246 (2001).
28. Yoon, M. *et al.* Heteropoly acid-incorporated TiO_2 colloids as novel photocatalytic systems resembling the photosynthetic reaction center. *J. Phys. Chem. B* **105**, 2539–2542 (2001).
29. Park, H. & Choi, W. Photoelectrochemical investigation on electron transfer mediating behaviors of polyoxometalate in UV-illuminated suspensions of TiO_2 and Pt/TiO_2. *J. Phys. Chem. B* **107**, 3885–3890 (2003).
30. Kim, H. N., Kim, T. W., Kim, I. Y. & Hwang, S.-J. Cocatalyst-free photocatalysts for efficient visible-light-induced H_2 production: Porous assembly of CdS quantum dots and layered titanate nanosheets. *Adv. Funct. Mater.* **21**, 3111–3118 (2011).
31. Kim, T. W. *et al.* Heterostructured visible light active photocatalyst of porous chromia nanoparticle-layered titanate nanohybrid. *Adv. Funct. Mater.* **17**, 307–314 (2007).
32. Kim, T. W. *et al.* Unique phase transformation behavior and visible light photocatalytic activity of titanium oxide hybridized with copper oxide. *J. Mater. Chem.* **20**, 3238–3245 (2010).
33. Kim, T. W., Hwang, S.-J., Park, Y., Choi, W. & Choy, J.-H. Chemical bonding character and physicochemical properties of mesoporous zinc oxide-layered titanate nanocomposites. *J. Phys. Chem. C* **111**, 1658–1664 (2007).
34. Hur, S. G. *et al.* Heterostructured nanohybrid of zinc oxide-montmorillonite clay. *J. Phys. Chem. B* **110**, 1599–1604 (2006).
35. Condon, J. B. Surface Area and Porosity Determinations by Physisorption: Measurements and Theory, 1st ed; Elsevier: Amsterdam; Boston, p.274 (2006).
36. Allen, T. *Powder Sampling and Particle Size Determination,* 1st ed; Elsevier: Amsterdam; Boston, p.660 (2003).
37. Arco, M. D., Galiano, M. V. G., Rives, V., Trujillano, R. & Malet, P. Synthesis and characterization of new Mg_2Al-Paratungstate layered double hydroxides. *Inorg. Chem.* **43**, 375–384 (2004).

Acknowledgements

This research is supported by the Core Technology of Materials Research and Development Program of the Korea Ministry of Intelligence and Economy (grant No. 10041232), by Korea Ministry of Environment as "Converging Technology Project" (191-101-001), and by National Research Foundation of Korea Grant funded by the Korean Government (2010-0001485). The experiments at PAL were supported in part by MOST and POSTECH.

Author contributions

S.-J.H. contributed to the conception and design of the experiment, analysis of the data and writing the manuscript. J.L.G. carried out design, synthesis and characterization of Zn-Cr-LDH-POM nanohybrid materials. T.W.K., I.Y.K. and J.M.L. designed photocatalytic experiments and established photofunctional mechanism for nanohybrids. All authors contributed to discussion, analysis of results and preparation of manuscript.

Additional information

Supplementary information accompanies this paper at http://www.nature.com/scientificreports

Competing financial interests: The authors declare no competing financial interests.

How to cite this article: Gunjakar, J.L., Kim, T.W., Kim, I.Y., Lee, J.M. & Hwang, S.-J. Highly Efficient Visible Light-Induced O_2 Generation by Self-Assembled Nanohybrids of Inorganic Nanosheets and Polyoxometalate Nanoclusters. *Sci. Rep.* **3**, 2080; DOI:10.1038/srep02080 (2013).